A Terramechanics-based Dynamic Model for Motion Control of Unmanned Tracked Vehicles

Ruizeng Zhang, Wei Zhou, *Senior Member, IEEE*, Haiou Liu, Jianwei Gong, *Member, IEEE*, Huiyan Chen and Amir Khajepour, *Member, IEEE*

Abstract—Existing terramechanics-based dynamic models for tracked vehicles (TRVs) are widely used in dynamics analysis. However, these models are incompatible with model-based controller design due to their high complexity and computational costs. This study presents a novel and simplified terramechanics-based dynamic model for TRVs that can be used in optimization-based real-time motion controller design. To this end, we approximated the track-ground interactions with an averaged term of the track-ground shear stresses to make the model computationally efficient and linearizable. By introducing the concepts of slip ratio and slip angle in the field of wheeled vehicles, the terramechanics-based dynamic model was finally simplified into a compact and practical single-track dynamic model reducing the demand for precise slip ratio measurements. The single-track model enables us to design an efficient motion control scheme by considering lateral and longitudinal dynamics separately. Finally, the proposed dynamic model was verified and validated under various road conditions using a real TRV. Additionally, the performance of different models was compared in simulation as an example to demonstrate that the proposed model outperforms the existing ones in TRV path-following tasks.

Index Terms—Autonomous vehicles, motion control, dynamic model, model predictive control

I. INTRODUCTION

Tracked vehicles (TRVs) are widely used in agriculture, construction, mining, military, and disaster relief operations [1]–[4]. Due to their superior ground adaptability [5], [6], TRVs typically operate on rough terrain to perform heavy-duty tasks. However, they are noisy and challenging to operate, imposing heavy physical and mental burdens on human drivers. With advancements in autonomous driving technology, the demand for unmanned TRVs has emerged, which is not only for safety concerns but also to deal with the labor shortage. In response, this paper proposes a novel dynamic model and an *autonomous* control scheme for TRVs to achieve optimal motion control performance.

Dynamic model-based motion planning and control methods have proven effective in the field of wheeled vehicles (WVs)

[7]–[10], but they face significant challenges when applied to TRVs. The primary obstacle in designing an efficient and effective model-based controller for TRVs is the absence of a ready-made control-applicable vehicle-ground interaction model [11], [12], comparable to the magic formula [13] or the UniTire model [14] used for WVs. Typically, modeling the track-ground interaction involves using numerical integration techniques to calculate driving and resistance forces on the track-ground contacting area based on the terramechanics theory [15]. Although lots of experimental data [16] has validated the accuracy of this approach, the numerical integration model is computationally expensive and impractical for model-based control methods, such as model predictive control (MPC), for the gradient of the model is difficult to calculate. Consequently, the terramechanics-based dynamic model is seldom used in real-time control. As an alternative, the kinematic model [17]–[19] and empirical model [20] are commonly used in motion control of TRVs due to their simplicity. However, the shortcomings of the both models are obvious. The kinematic model struggles to deal with dynamics-related constraints which are crucial for driving safety, especially in high-speed or off-road scenarios. As for empirical models, they do not accurately reflect the real mechanisms of turning [21]. Moreover, some parameters do not have specific physical meaning and must be obtained through real car tests. Therefore, an effective dynamic model that balances accuracy and complexity is urgently needed for the motion control of TRVs.

In this paper, we aim to develop a simplified but accurate single-track dynamic model for TRVs, suitable for model-based control methods, akin to the bicycle model for WVs [22], [23]. TRVs change the torques on both sides of tracks to alter their heading and velocity simultaneously, resulting in a strong dynamic coupling between lateral and longitudinal directions [24]. Consequently, the dynamics of TRVs differ significantly from those of WVs, although certain commonalities can be found to enable us to simplify the dynamic model of TRVs into a single-track one. As previously mentioned, terramechanics-based dynamic models are accurate and well-validated but complex; therefore, we are considering if we can simplify the terramechanics-based dynamic models while maintaining their accuracy. Fortunately, our mathematical derivations and experimental evidence indicate that this is feasible.

Typically terramechanics-based dynamic analysis ideally simplifies the track-ground pressure as uniformly distributed [21], which is counterfactual to experimental results – the track-ground pressure is concentrated underneath the road
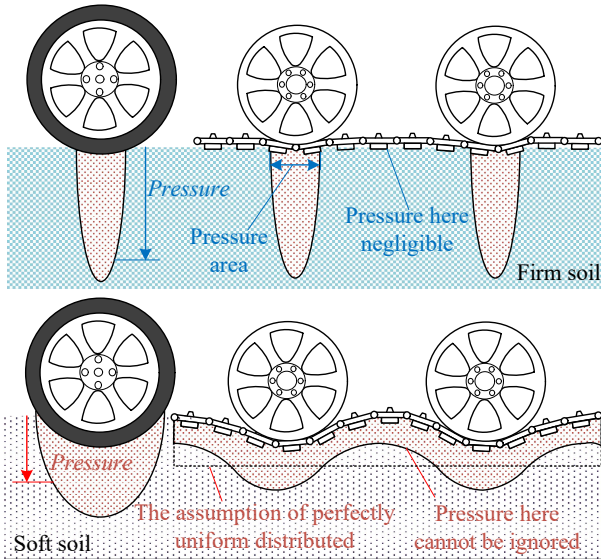
Fig. 1. Comparision of wheel/track-ground pressure on different soils.

wheels on firm ground. The firmer the ground is, the more concentrated the pressure becomes [25]. As illustrated in Fig. 1, the track-ground pressures of TRVs are similar to tire-ground pressure on firm ground but more dispersed on soft soil. Inspired by [26]–[28], we developed a track-ground contact model for firm ground that avoids integrals, making it more practical in real-time controller design. In our model, the track-ground pressure is assumed to be concentrated in a small area underneath the road wheels; thus, it is reasonable to use the states of the center point to approximate the states of the entire area. This approximation avoids the complex integration while maintaining accuracy, which makes terramechanics-based theory practically tractable in optimization-based real-time control for path-following.

The main contributions of this work are presented below:

1) We develop a novel and simplified single-track dynamic model for TRVs on firm ground, suitable for model-based control techniques in real-time. This model enables the application of terramechanics-based methods in the real-time control of TRVs.
2) We propose a coordinated control scheme for TRVs' longitudinal and lateral motion control, which satisfies path-tracking performance with low computational complexity.
3) We verify the proposed dynamic model through real-car experiments and validate the proposed path-following controller via multibody dynamics simulations.

This paper is organized as follows. Section II analyzes related work and points out the shortcomings of existing works. Section III presents the proposed TRV dynamic model. Section IV describes the control scheme of longitudinal and lateral dynamics and the MPC algorithm formulations. Section V discusses the real vehicle experiment results of model verification, and simulation results in path-following tasks. Finally, the conclusions and scope for future works are summarized in Section VI.

II. RELATED WORK

To summarize relevant prior work and illustrate its short-comings, related work will be discussed from two aspects: modeling and controlling.

A. Modeling of TRVs

Existing literature for TRV motion modeling is primarily based on four types of models: kinematic models [17]–[19], pure friction models [5], [29], empirical models [20] and the terramechanics-based models [21], [30], [31].

Kinematic models are simple and adaptable, which could handle most well-defined scenarios; thus, these models are widely used in both small low-speed TRVs [6], [32] and large high-speed TRVs [18], [19]. However, kinematic models may fail when the dynamics-related information dominates control performance. For example, adhesion constraints and actuator constraints are crucial for safely following a desired path with curves at a high speed. In addition, kinematic model-based control methods are generally require a parameter estimation algorithm [18]. For instance, Zhao et al. [17] propose a kinematics-aware MPC algorithm that estimates six linear slip parameters with an extended Kalman filter (EKF). Besides, kinematic controllers usually combine with a simplified lower controller to generate the desired kinematic variable. The quality of the lower controller would influence the overall system performance significantly. Despite these disadvantages, the kinematic model remains the most widely used model for motion control of TRVs among existing models.

Pure friction models assume turning resistance coefficient is a constant, which is applicable for small TRVs on hard surface but not for large TRVs on deformable soil. Therefore, empirical models are employed to address this issue. For example, the Nikitin empirical formula [20] describes the relationship between the turning resistance coefficient and the turning radius. This formula is one of the most widely used models for estimating turning resistance [33], [34]. However, the Nikitin empirical formula also fails to depict the lateral velocity, because it assumes the offset of the turning center is zero. That is, there is no lateral velocity on the center of gravity (CoG). Additionally, it assumes the turning resistance coefficient is independent of vehicle velocity, which is incorrect.

Finally, terramechanics theory is based on the track-ground interaction mechanism and can calculate track-ground forces accurately. As a result, the terramechanics theory is popular in TRV dynamics analysis [16], [21], [30], [31]; however, this model is incompatible with online model-based control algorithms such as MPC or linear quadratic regulator (LQR). Terramechanics-based theories rely on shear stress-shear displacement relationship [35]–[37] to make accurate analysis for TRV performance evaluation, rather than for path-following control tasks. The use of tracks not only disperses the wheel-ground pressure and generates higher adhesion forces, but also makes the interaction between vehicle and ground extremely complex [38]. Integration is embedded in the terramechanics-based models to obtain highly accurate models which are

over-complicated for online control methods. Therefore, despite their high accuracy, the terramechanics-based models are rarely used for path-following controller design.

In summary, existing models for TRVs are either oversimplified or too complex to be applied to optimization-based real-time control. Therefore, it is necessary to propose a simplified but accurate dynamic model for path tracking of TRVs.

B. Motion Control of TRVs

A brief survey on existing motion control algorithm for TRVs is provided as a supplement. As is shown in Table I, existing motion control algorithms for autonomous TRVs can be roughly divided into three categories: state error feedback control, geometry-based control, and optimization-based control.

TABLE I
PATH TRACKING ALGORITHM OF TRVS COMPARISON

Categories	Algorithm	Application	Verification
State error feedback control	PID [39]–[42] SMC [43] Fuzzy control [44]–[46] Adaptive control [47] Linear feedback control [48], [49], [50]–[52]	Small TRVs [39], [40], [41], [43], [48], [46], [50] Large TRVs [49], [42], [45], [47], [52] Sea mining TRV [44] Unspecified [51]	Real car [40], [41], [46] Simulation [39], [43], [48], [49], [42], [44], [47], [45], [50]–[52]
Geometry-based control	Pure pursuit [53] Stanley algorithm [54]	Small TRVs [53], [54] Large TRVs	Real car [53] Simulation [54]
Optimization-based control	LQR [55] MPC [56]–[61]	Small TRVs [55], [57] Large TRVs [59], [60] Sea mining TRVs [56] Agriculture TRVs [58] Unspecified [61]	Real car [57], [59]–[61] Simulation [56], [55], [58]

Among the algorithms investigated, state error feedback control and optimization-based control are widely used for the path tracking of TRVs. The state error feedback control is often used in the early stages of the autonomous driving technology, due to its low computational complexity and minimal requirements for vehicle models. However, these models are not good at handling multiple constraints on multiple states, which is important to driving safety. As a type of optimization-based control algorithm, MPC achieves the optimal cost over a finite horizon by comprehensively considering control objectives, predictive states, and constraints. Despite its effectiveness in tracking control, MPC requires an accuracy model to ensure the control performance, but the model cannot be overly complex to maintain real-time performance. Thus, the balance between the model complexity and accuracy is critical. For MPC of TRV, the main issue is the lack of a ready-made model that meets MPC requirements.

The above conclusions is supported by the statistics on the algorithms in Table I. Among 14 articles using the state error

feedback control method, only three of them are verified with real cars. Furthermore, all the three articles are verified using small TRVs and model-free control algorithms like PID and fuzzy control. Therefore, the real performance of the state error feedback control method on large TRVs has not been well verified. Optimization-based tracking control, especially the MPC algorithm, has considerable real car applications on both small TRVs and large TRVs. However, most works verified with real cars are based on the kinematic model. In these cases, the sprocket speeds on both sides are virtual control variables, implemented by the lower controller such as a motor controller. The disadvantages of kinematic models have been discussed in the section II-A. Thus, the analysis of existing related works supports our view that a simplified but accurate dynamic model for path tracking of TRVs is urgently needed.

III. TRACKED VEHICLE DYNAMIC MODEL

As mentioned previously, the proposed dynamic model for TRVs is suitable for firm ground, where the track-ground normal force concentrates in a limited area underneath the road wheel; therefore, some equivalent simplification can made to avoid the numerical integral process.

A. Track-ground Interaction

1) Full Vehicle Dynamics: The TRV's whole dynamics are shown in Fig. 2, consisting of the longitudinal, lateral, and yaw dynamics in the vehicle body coordinates $x - o - y$ under global ground coordinates $X - O - Y$. The $x_w - o_w - y_w$ coordinates are fixed on the track underneath the wheel center (the zoomed part in Fig. 2). The shaded area surrounded by a dashed line represents the pressure area.
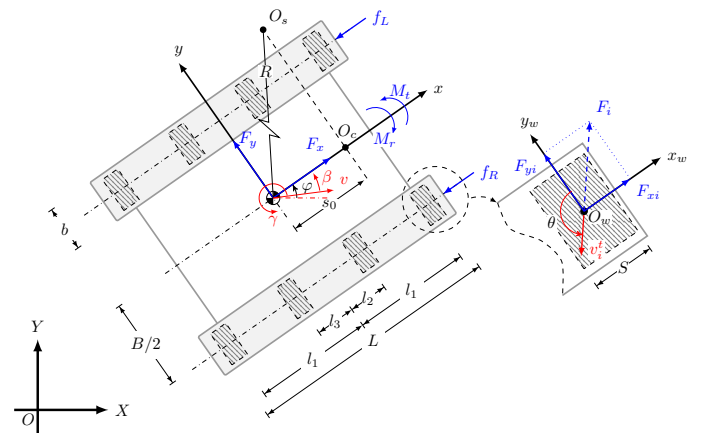

Fig. 2. Illustration of dynamics for dual-track TRVs.

In Fig. 2, R and O_s represent the radius of the instant turning trajectory and the instant turning center, respectively. O_c is the projection of O_s on the x-axis, and s_0 is the distance between O_c and the center of gravity (CoG). φ is the yaw angle between X-axis and x-axis, β is the chassis slip angle, and γ is the yaw rate. B is track center distance. L and b are track-ground contact length and width, respectively. l_i is the distance between road wheel centers and the vehicle's CoG with subscripts i as the ith road wheel. f is the driving

resistance. The resultant longitudinal and lateral forces F_x and F_y act on the CoG of the vehicle. For TRVs, lateral shear forces on both tracks impede vehicle turning, and the corresponding influence acts on the CoG, resulting in a resistance moment M_r. Similarly, longitudinal shear forces promote vehicle turning and obtain a driving moment M_t. The force applied on the track below i^{th} road wheel F_i with an opposite direction of the track-ground shear velocity v_i^t is decomposed into longitudinal force ($F_{x,i}$) and lateral force ($F_{y,i}$). θ is the angle between axis-y_w and v_i^t. S is the length of the normal pressure zone in the longitudinal direction, and its side view is shown in Fig. 3 (b).

According to Newton's second law, the TRV's dynamic model can be formulated as

$$\dot{v}_y = -v_x\gamma + \frac{1}{m}\sum_{i=1}^{n}\left(F_{y,i}^{\text{R}} + F_{y,i}^{\text{L}}\right) \tag{1a}$$

$$\dot{v}_x = v_y\gamma + \frac{1}{m}\sum_{i=1}^{n}\left(F_{x,i}^{\text{R}} + F_{x,i}^{\text{L}}\right) \tag{1b}$$

$$\dot{\gamma} = \frac{1}{I_z}\left(\frac{B}{2}\sum_{i=1}^{n}\left(F_{x,i}^{\text{R}} - F_{x,i}^{\text{L}}\right) - \sum_{i=1}^{n}\left(l_i F_{y,i}^{\text{R}} + l_i F_{y,i}^{\text{L}}\right)\right) \tag{1c}$$

where superscripts 'L' and 'R' denote the left and right sides, n is the total number of wheels on one side, m is the vehicle mass, I_z is the moment of inertia.

2) Track-ground Interaction: Janosi-Hanamoto's equation (Eq. 2) [35] is employed as the shear stress-shear displacement model due to its concise form and broad applicability.

$$\tau = (c + p\tan\varphi)\left(1 - e^{-j/K}\right) \tag{2}$$

where τ is the shear stress, K is the shear deformation parameter, and c and p are the cohesion and normal pressures, respectively. When the soil is non-cohesive, the Eq. (2) can be rewritten as

$$\tau = p\mu\left(1 - e^{-j/K}\right) \tag{3}$$

with μ the coefficient of shear.

Fig. 3 (a) shows the distribution of longitudinal shear stress τ_x when considering uniform track-ground pressure. Points A and B are the front end of the track-ground contact area and a certain point fixed on the track, respectively. d represents the distance between points A and B. When the vehicle drives forward, point B moves backward relative to the vehicle starting from point A, and the track shears the soil with a velocity of v^t during this process, where superscript t denotes track. The process takes time $t^t = \frac{d}{\omega r}$. r and ω present the sprocket pitch circle radius and speed, respectively. The shear displacement $j = v^t \cdot t^t$. v_x represents the longitudinal velocity of CoG. In traditional terramechanics-based methods for TRV dynamic analysis, track-ground pressure is considered to be uniformly distributed. When calculating the shear displacement j, the shear velocity v^t is generally assumed to be unchanged. That is, the vehicle states remain unchanged for a long time. Thus, this method [21] can only handle the steady-state turning scenario.
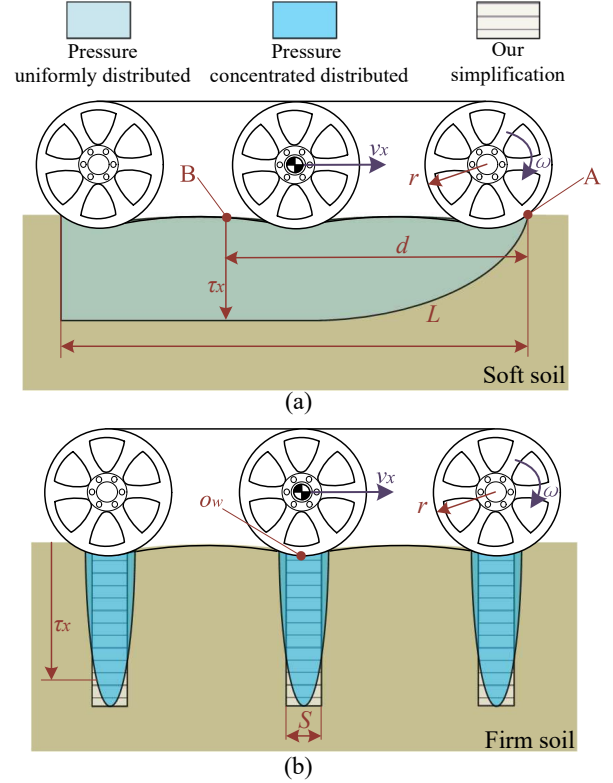

Fig. 3. Longitudinal shear stress distribution with (a) uniformly distributed and (b) concentrated distributed normal pressure distribution assumption.

Our experimental results (Fig. 10) show that the track-ground pressure concentrates in a small area underneath the road wheels on firm but deformable ground. Fig. 3 (b) illustrates the shear stress distribution when the track-ground pressure is concentrated in a small area. This finding allows us to significantly simplify the terramechanics-based dynamic models for TRVs. On the one hand, only a small pressure area needs to be integrated, thus it is reasonable to assume that the vehicle states remain steady for a short period. This allows us to extend traditional terramechanics-based methods to a generalized situation rather than only steady-state turning. On the other hand, integration can be avoided by using an approximate alternation. Specifically, o_w in Fig. 2 is the center point of the pressure area. Thus, its velocity is the average velocity of the points in the pressure area while keeping the shear time of o_w as the average time. Therefore, point o_w possesses the average shear displacement of all the points in the pressure area. Then, the average shear displacement can be used to calculate the shear force over the entire region without integration. The velocity of the point o_w relative to the ground in the body coordinate system can be obtained as following:

$$v_{x,i}^t = v_{x,i} - rw \tag{4a}$$

$$v_{y,i}^t = v_{y,i} \tag{4b}$$

$$v_i^t = \sqrt{v_{x,i}^t{}^2 + v_{y,i}^t{}^2} \tag{4c}$$

where $v_{x,i}$ and $v_{y,i}$ are the velocity of the ith wheel center in x and y directions, and their combined velocity is v_i. The shear

time t_i^t and shear displacement j_i of our simplified model can be obtained:

$$t_i^t = \frac{S}{2rw} \tag{5}$$

$$j_i = v_i^t \cdot t_i^t = \frac{S}{2}\sqrt{\left(\frac{v_{y,i}}{rw}\right)^2 + \left(\frac{v_{x,i} - rw}{rw}\right)^2} \tag{6}$$

where t_i^t is the average shear time of all elements in the pressure area S in Fig. 3 (b) and j_i is the average shear displacement. It should be noted that we do not know the exact value of S, but it remains constant when the road conditions are unchanged. Fortunately, it is unnecessary to calculate the exact value of S because S and shear deformation parameter K will form a new parameter C_1 in Eq. (9a), which can be obtained experimentally.

3) Introducing Slip Ratio and Slip Angle: Referring to the concept of tire slip angle in the WVs' dynamic model, let the slip angle α and slip ratio λ of the track under each road wheel be

$$\tan\alpha_i = -\frac{v_{y,i}}{v_{x,i}} \tag{7a}$$

$$\lambda_i = \frac{rw - v_{x,i}}{v_{x,i}} \tag{7b}$$

$$j_i = \frac{S}{2}\sqrt{\lambda_i^2/(1+\lambda_i)^2 + (\tan\alpha_i)^2/(1+\lambda_i)^2} \tag{7c}$$

According to terramechanics theory [16], [21] and Eq. (3), the average shear stress and its component in longitudinal and lateral direction under the ith road wheel can be obtained as

$$\tau_i = p\mu\left[1 - e^{-\frac{C_1 s}{1+\lambda_i}}\right] \tag{8a}$$

$$\tau_{x,i} = \frac{\lambda_i}{s}\tau_i \tag{8b}$$

$$\tau_{y,i} = \frac{\tan\alpha_i}{s}\tau_i \tag{8c}$$

where C_1 is coefficient with $C_1 = S/(2K)$. Parameter s can be formulated as $s = \sqrt{\lambda_i^2 + (\tan\alpha_i)^2}$. Then, considering the average pressure area under a single road wheel, the track-ground force can be obtained as

$$F_i = F_{z,i}\mu\left[1 - e^{-\frac{C_1 s}{1+\lambda_i}}\right] \tag{9a}$$

$$F_{x,i} = \frac{\lambda_i}{s}F_i \tag{9b}$$

$$F_{y,i} = \frac{\tan\alpha_i}{s}F_i \tag{9c}$$

Fig. 4 illustrates the effect of longitudinal slip ratio on lateral shear stress. Slip ratio λ and slip angle α are assumed to be proportional to demonstrate the influence of λ. It can be seen that when the slip ratio is relatively small, i.e., when the turning radius is relatively large, neglecting λ has a limited impact on model accuracy. However, when the turning radius is small, neglecting λ results in a lateral shear stress that is larger than the actual value. Related research [62], and our experimental results show the turning radius is less than 5 and 10 meters when $\lambda = 10\%$ and $\lambda = 5\%$ on rural dirt roads, respectively. Thus, the slip ratio λ should be considered for TRVs to ensure the performance during sharp turns.
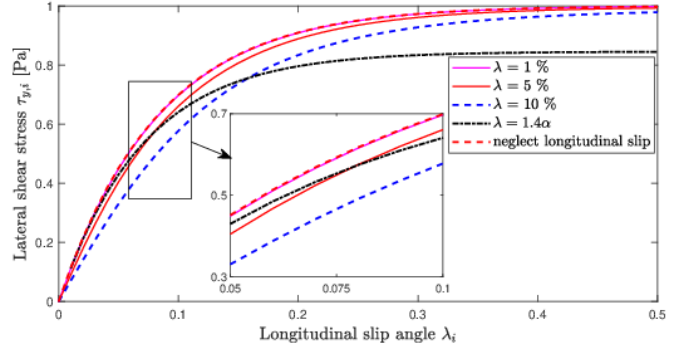

Fig. 4. Influence of longitudinal slip on lateral shear stress when $p\mu = 1$.

Equations (1)-(9) provide a dynamic model for TRVs based on the terramechanics theory. By introducing slip angle α and slip ratio λ, we find the proposed track-ground model and the tire model of the wheeled vehicle, especially the UniTire model [14], share some consistency in form. This indicates a certain commonality in the interaction between ground and vehicle.

B. Single-track Dynamic Model

The dual-track model must consider the states of all the wheels, which for a TRV typically means at least eight wheels simultaneously. The slip ratio λ measure relies on accurate longitudinal velocity, but this is difficult to obtain for TRVs. Based on our experience, the yaw rate measured by the inertial measurement unit (IMU) is more accurate, as vibration has a limited effect on rotation states measurement. Thus, we can calculate the overall slip velocity using the measured yaw rate:

$$v_x^{t,R} - v_x^{t,L} = \left(\omega^R - \omega^L\right)r - B\gamma_{\text{mea}} \tag{10}$$

where, γ_{mea} is yaw rate measured by IMU. And the average shear velocity $v_x^{t,\text{ave}}$ can be

$$v_x^{t,\text{ave}} = \frac{v_x^{t,R} - v_x^{t,L}}{2} \tag{11}$$

By substitute the shear velocity $r\omega - v_{x,i}$ in Eq. 7 with the average one $v_x^{t,\text{ave}}$, the lateral forces on the ith wheel can be written as:

$$F_{y,i}^L = -\frac{v_{y,i}}{\sqrt{v_{y,i}^2 + \left(v_x^{t,\text{ave}}\right)^2}}F_{z,i}^L\mu\left[1 - e^{-\frac{C_1\sqrt{v_{y,i}^2 + \left(v_x^{t,\text{ave}}\right)^2}}{v_x^L - v_x^{t,\text{ave}}}}\right] \tag{12a}$$

$$F_{y,i}^R = -\frac{v_{y,i}}{\sqrt{v_{y,i}^2 + \left(v_x^{t,\text{ave}}\right)^2}}F_{z,i}^R\mu\left[1 - e^{-\frac{C_1\sqrt{v_{y,i}^2 + \left(v_x^{t,\text{ave}}\right)^2}}{v_x^R + v_x^{t,\text{ave}}}}\right] \tag{12b}$$

where, $v_x^L = v_x - \frac{B}{2}\gamma_{\text{mea}}$ and $v_x^R = v_x + \frac{B}{2}\gamma_{\text{mea}}$.

Inspired by the bicycle model for wheeled vehicles, we simplified the dual-track model to a single-track model (Fig. 5). In this model, we assume an imaginary full-weight track located in the center of the TRV. Generally, the torque difference between the tracks on both sides drives the vehicle to turn.

However, there is no such torque difference in single-track model. Thus, an imaginary driving moment M_t is applied on the single-track model to drive the vehicle to turn.
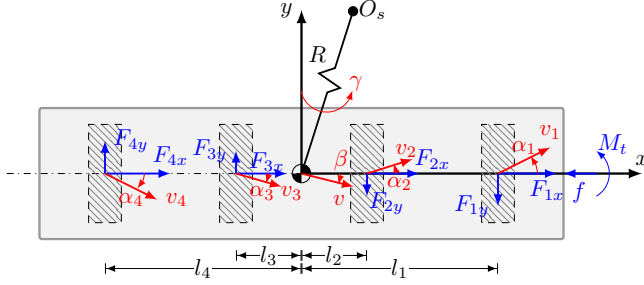

Fig. 5. Single-track tracked vehicle model.

The imaginary track should exhibit similar dynamics to the double-track model. Thus, the lateral force of the ith wheel in the imaginary track can be formulated as:

$$
F_{y,i}^{\text{IMG}} = -\frac{v_{y,i}}{\sqrt{v_{y,i}^2 + \left(v_x^{t,\text{ave}}\right)^2}} F_{z,i}\mu \left[1 - \frac{F_{z,i}^L}{F_{z,i}} e^{-\frac{C_1\sqrt{v_{y,i}^2 + \left(-v_x^{t,\text{ave}}\right)^2}}{v_x^L - v_x^{t,\text{ave}}}} \right.
$$
$$
\left. - \frac{F_{z,i}^R}{F_{z,i}} e^{-\frac{C_1\sqrt{v_{y,i}^2 + \left(v_x^{t,\text{ave}}\right)^2}}{v_x^R + v_x^{t,\text{ave}}}} \right]
\tag{13}
$$

According the following limit equation:

$$
\lim_{\Delta x \to 0} \frac{F_{z,i}^L}{F_{z,i}} f(x - \Delta x) + \frac{F_{z,i}^R}{F_{z,i}} f(x + \Delta x) = f(x)
\tag{14}
$$

The $F_{y,i}^{\text{IMG}}$ can be approximated as Equation(15), when $\left(\frac{B}{2}\gamma + v_x^{t,\text{ave}}\right)$ is small compared with v_x, that is, when the turn radius is not over small. It should be noted that a similar simplification is also made in the bicycle model for WVs, but the average shear velocity $v_x^{t,\text{ave}}$ of TRVs is bigger than WVs. The impacts of the simplification will be discussed in the experimental results section.

$$
F_{y,i}^{\text{IMG}} = -\frac{v_{y,i}}{\sqrt{v_{y,i}^2 + \left(v_x^{t,\text{ave}}\right)^2}} F_{z,i}\mu \left[1 - e^{-\frac{C_1\sqrt{v_{y,i}^2 + \left(v_x^{t,\text{ave}}\right)^2}}{v_x}} \right]
\tag{15}
$$

Based on the above derivation, a more compact single-track model for TRVs is formulated as

$$
\dot{v}_y = -v_x\gamma + \frac{1}{4}g\mu \sum_{i=1}^{n} \left[\frac{v_{y,i}}{\sigma_i} \left(1 - e^{-\frac{C_1\sigma_i}{v_x}} \right) \right]
\tag{16a}
$$

$$
\dot{\gamma} = \frac{M_t}{I_z} - \frac{mg\mu}{4I_z} \sum_{i=1}^{n} \left[l_i \frac{v_{y,i}}{\sigma_i} \left(1 - e^{-\frac{C_1\sigma_i}{v_x}} \right) \right]
\tag{16b}
$$

where, $\sigma_i = \sqrt{v_{y,i}^2 + \left(v_{x,i}^{t,\text{ave}}\right)^2}$, M_t is the driving moment, which promotes vehicle turning and can be used to calculate the sprocket torques which are the final control outputs. Thus, this model enables us to divide the sprocket torques into the velocity sustain and turning parts so that the TRV dynamics can be decoupled into longitudinal and lateral directions.

It should be noted that a single-tracked TRV does not exist in the real world, as it cannot perform turning maneuvers; however, it is reasonable to simplify the model of TRVs into a single-tracked one because the single-track model captures the most essential vehicle-ground dynamic features. Although the input M_t cannot be applied on a single-tracked TRV by the single-tracked TRV itself in the reality, we can calculate the required input using the single-track model and implement it using a dual-track TRV in dynamic control.

Considering vehicle position states, the following equations can be derived:

$$
\dot{\varphi} = \gamma
\tag{16c}
$$

$$
\dot{X} = v_x \cos(\varphi) - v_y \sin(\varphi)
\tag{16d}
$$

$$
\dot{Y} = v_x \sin(\varphi) + v_y \cos(\varphi)
\tag{16e}
$$

By defining $\boldsymbol{\xi} = [v_y\ \gamma\ \varphi\ X\ Y]^{\mathsf{T}}$ as the state vector, the turning driving moment M_t as the manipulated variable, and $\boldsymbol{y} = [v_y\ \gamma\ \varphi\ X\ Y]^{\mathsf{T}}$ as the outputs of the system, the Eq. (16) can be linearized at operation point in the state-space representation as:

$$
\dot{\tilde{\boldsymbol{\xi}}} = \boldsymbol{A}\tilde{\boldsymbol{\xi}} + \boldsymbol{B}\tilde{M}_t
\tag{17a}
$$

$$
\tilde{\boldsymbol{y}} = \boldsymbol{C}\tilde{\boldsymbol{\xi}},
\tag{17b}
$$

where, $\tilde{\boldsymbol{\xi}} = \boldsymbol{\xi} - \boldsymbol{\xi}_0, \tilde{\boldsymbol{y}} = \boldsymbol{y} - \boldsymbol{y}_0, \tilde{M}_t = M_t - M_{t0}$. Matrix $\boldsymbol{A}$, $\boldsymbol{B}$ and $\boldsymbol{C}$ denote state, input-to-state and state-to-output matrix, respectively.

By using Euler's approximation, Eq. (17) can be discretized at sample time t_s, and the discrete-time state-space equation can be obtained as follows:

$$
\tilde{\boldsymbol{\xi}}(k+1) = \boldsymbol{A}_d\tilde{\boldsymbol{\xi}}_d(k) + \boldsymbol{B}_d\tilde{M}_t(k)
\tag{18a}
$$

$$
\tilde{\boldsymbol{y}}(k) = \boldsymbol{C}_d\tilde{\boldsymbol{\xi}}(k)
\tag{18b}
$$

where $\boldsymbol{A}_d = \boldsymbol{A}t_s + \boldsymbol{I}$, $\boldsymbol{B}_d = \boldsymbol{B}t_s$ and $\boldsymbol{C}_d = \boldsymbol{C}$.

C. The single-track model VS the full dynamic model

Although the full dynamic model is theoretically more accurate and has more degrees of freedom than the single-track model, it is not easy to employ in real-world motion control of TRVs.

Firstly, the full dynamic model is more computationally complex. The full dynamic model for an 8-wheeled TRV needs to do 32 times exponential operations per iteration, while the single-track model only requires 8 times. Running the full dynamic model one million times on an Intel Core i7-12800H computer takes around 0.526 seconds, whereas the single-track model takes only 0.146 seconds.

Secondly, the full dynamic model relies on an accurate slip ratio on both sides to ensure its performance. However, accurate estimating the slip ratio is challenging. It requires a high-precision IMU and complex estimation methods, and is also affected by terrain undulations. The slip ratio is generally calculated by comparing the vehicle velocity and track speed; however, this method introduce errors on uneven terrain, even with an accurate IMU. As shown in Fig. 6, when the vehicle drives a distance in blue, the track travels a longer distance

in red, but slip actually does not happen. Fortunately, the single-track model replaces the need for an accurate slip ratio measurement with an average slip $v_x^{t,\text{ave}}$ in Eq. (10-11), reducing the requirements on the measurement system and mitigating the problem. The average slip calculated by yaw rate is more reliable because the yaw rate is less affected by vibration. Additionally, the average slip uses the differential of track speed on both sides rather than the track speed itself, so that mitigates the effects of terrain undulations.
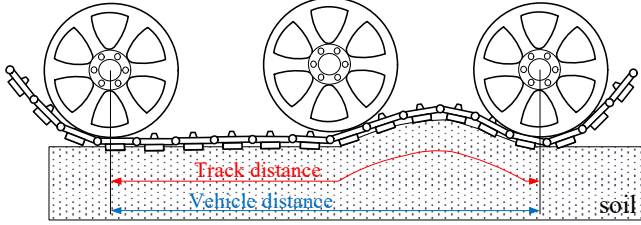

Fig. 6. Effect of terrain undulations on slip ratio.

Thirdly, the off-road environment TRVs travel on are often uneven, and road profiles are generally unmodeled or unmeasured. MPC does not perform well with unmodeled disturbances. Therefore, it is wise to ignore longitudinal dynamics in MPC and instead use a high-frequency feedback controller.

In summary, compared to the full dynamic model, the single-track model benefits from lower computational complexity, reduced measurement demands, and less sensitivity to terrain roughness, making it more practical for real-world applications.

IV. CONTROLLER DESIGN FOR TRACKED VEHICLES

A. Longitudinal and Lateral Coordinated Control Scheme

For TRVs, the longitudinal and lateral dynamics are coupled. In this section, a longitudinal and lateral coordinated control scheme is proposed, as shown in Fig. 7.
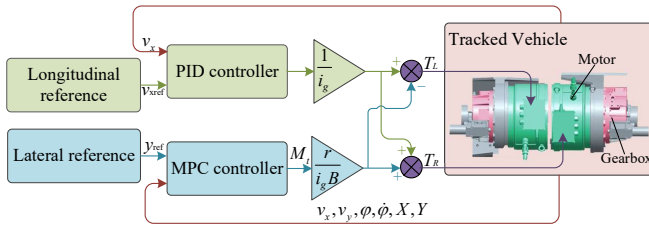

Fig. 7. Longitudinal and lateral coordinated control scheme.

In this scheme, the driving moment M_t for turning is calculated through an MPC controller, and the driving force required to follow the longitudinal reference velocity v_{xref} is fulfilled by a PID controller. y_{ref} is the lateral reference. The torques of the motors on both sides, T_L and T_R, are calculated as control inputs for the dual-motor drive TRVs as Eq. (19).

$$T_L = T_{\text{longi}} - \frac{M_t r}{i_g B} \quad (19a)$$

$$T_R = T_{\text{longi}} + \frac{M_t r}{i_g B} \quad (19b)$$

where, i_g is the gear ratio of reducer, T_{longi} and T_{lat} are drive motor torque required for vehicle longitudinal travel and turning, respectively.
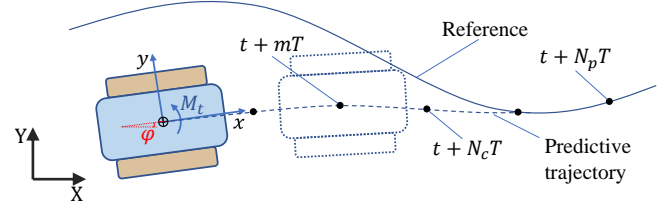
B. Nonlinear MPC Problem Formulation

Fig. 8. Path-following for TRVs.

The nonlinear MPC [63]–[65] is employed in this study to fulfill the TRV path following tasks. The controller should allow the unmanned TRV to track the desired path and yaw angle while keeping the vehicle states within the constraints. The single-track dynamic tracking model is nonlinear but can be linearized at the current state. Fig. 8 shows the reference and prediction in path-following for TRVs. The vehicle's longitudinal velocity is assumed to be constant during the prediction horizon as in [66]. Thus, the quadratic programming problem can be formulated as following:

$$\min_{M_t} \sum_{k=1}^{N_p} \left[\|y_d(k,t) - y_{\text{ref}}(k,t)\|_{\boldsymbol{Q}}^{\mathbf{2}} + \|M_t(k,t) - M_t(k-1,t)\|_{\boldsymbol{R}}^{\mathbf{2}} \right]$$
$$(20)$$

Subject to
$$\boldsymbol{\xi}(k+1) = \boldsymbol{A}_d \boldsymbol{\xi}(k) + \boldsymbol{B}_d M_t(k), \quad k = 0,1,2,\cdots,N-1$$
$$\boldsymbol{y}_d(k) = \boldsymbol{C}_d \boldsymbol{\xi}(k), \quad k = 0,1,2,\cdots,N-1,N$$
$$\boldsymbol{\xi}(0) = \boldsymbol{\xi}(t)$$
$$M_{t,\min} \leq M_t(k) \leq M_{t,\max}$$
$$\Delta M_{t,\min} \leq M_t(k) - M_t(k-1) \leq \Delta M_{t,\max}$$
where, $M_{t,\max}$ and $M_{t,\min}$ are the limits of the turning resistance. $\Delta M_{t,\max}$ and $\Delta M_{t,\min}$ denote the limits of turning resistance rate. In the cost function, the first term ensures the goal of path-following, and the other term penalizes the change of the driving moment M_t to avoid sharp turning. In addition, the Q and R are the positive semidefinite weight matrices for the path following and the control effort, respectively.

V. RESULTS AND ANALYSIS

This section demonstrates the effectiveness of the proposed model and path-following strategy using simulation and real-car experiments. The precision of the single-track model is verified through real car experimental results in steady-state turning situations. Subsequently, the control strategy in various scenarios is evaluated using MATLAB/Simulink and co-simulation with multibody dynamic software.

A. Real car model verification

The proposed dynamic model was verified on an electric-powered TRV under different road conditions. As shown in Fig. 9 (a), the TRV is driven by independent motors on both

sides, which can provide feedback on the speeds and torques. The vehicle is equipped with differential global positioning system (GPS) and an IMU to collect real-time vehicle trajectory and pose information. More than 100 groups of steady turning data are collected in a farm area in Hebei province, China, across various road types, including sand-grave road, firm dirt road, and cement road for model validation, as Fig. 9 (a)-(c) shown respectively. There was no precipitation for at least one week before data collection. The detailed parameters of the test TRV are listed in Table II.
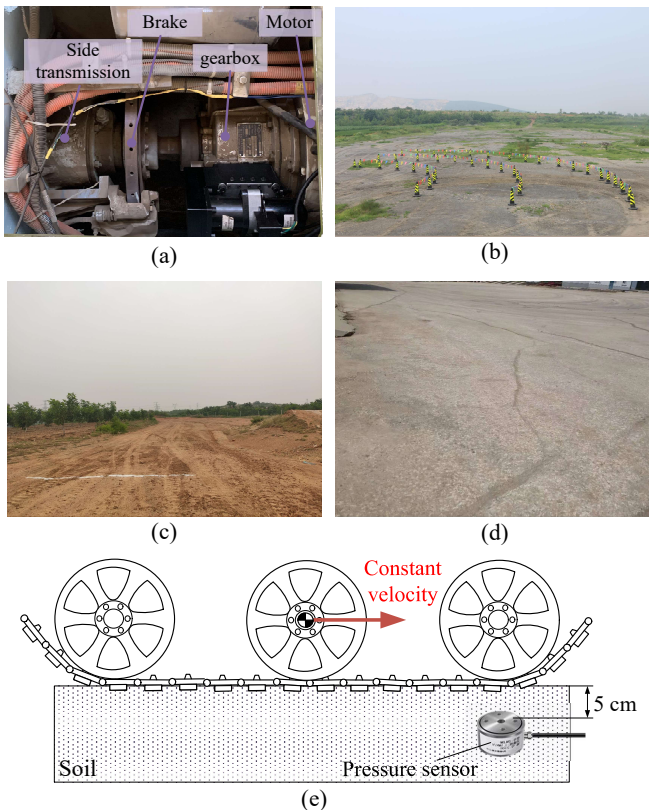

Fig. 9. (a) Transmission system in one side, (b) sand-gravel road, (c) firm dirt road, (d) cement road of the real vehicle experiment, (e) pressure measurement setup.

TABLE II
TEST RELATED PARAMETERS.

Parameter	Value/unit	Description
m	9660kg	Vehicle mass
B	2.464m	Track center distance
L	2.707m	Length of track contact ground
b	0.365m	Width of track contact ground
r	0.2654m	Sprocket pitch circle radius
n	4	Number of road wheel in single side
P	75kw	Rated power of single-side drive motor
$P_{\max}$	110kw	Maximum power of single-side drive motor
T_{err}	≤10Nm	Torque feedback error
P_{err}	≤15cm	GPS positioning error
I_z	15800kgm^2	Moment of inertia (estimated)

An essential step in the model derivation is the assumption that the normal pressure between the track and the ground is mainly concentrated in a limited area under the road wheels on

firm ground. To measure the track-ground pressure, a pressure sensor was buried about 5 cm underground ,allowing the tracks to roll over it at a constant speed, as Fig. 9 shows. The depth of 5 cm was chosen to avoid tracks crushing the sensor while ensuring sensitive measurement. After the measurements were taken, the time series of pressure signals were converted to space series via the constant vehicle velocity. Fig. 10 shows the experimental qualitative results of the track-ground pressure, indicating a multi-peak shape of the track-ground pressure with the peak occurs just below the center of the road wheel. The experimental results support our assumption that the track-ground pressure is mainly concentrated in a limited area beneath the road wheels.
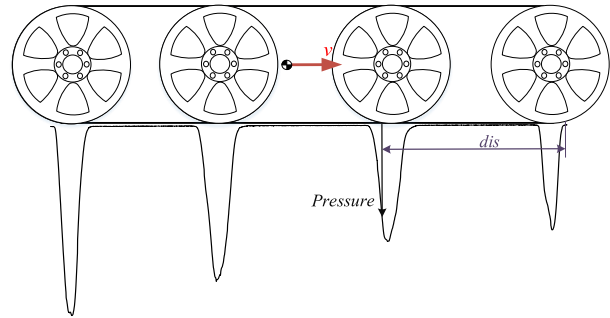

Fig. 10. Track-ground pressure experimental results.

The single-track model was validated in a steady-state turning process, where the vehicle velocity and yaw rate remain constant. The detailed collecting and validating process can be divided into 4 stages:

- Test site selection: We chose a place where the soil has uniform properties and the terrain is flat;
- Data collection: Constant sprocket speed commands on both sides were issued by a remote controller, enabling the test TRV to perform a steady-state turn. Vehicle states at various steering degrees, speeds and directions were collected, including position, sprocket speeds, and torques, velocity, and acceleration information;
- Data preprocess: Only continuous data with constant velocity and steering degree were selected. We then fitted the path of each piece of data with a circle and tagged the data with the circle's radius. Subsequently, the mean value of the vehicle state for each piece of data was calculated;
- Model validation: Finally, the proposed single-track model in Eq. (16) was validated using the mean value of each piece of data. The results are shown in Fig. 11 and 12.

We use the steady-state turning process to validate the model for two main reasons. Firstly, the validation focused on the interaction between the TRV and the ground. The primary difference between the proposed dynamic model and the existing TRV control models is the application of the terramechanics theory. The steady-state turning process ensures that the verification of track-ground interaction is not affected by changes in vehicle state. Secondly, Due to the
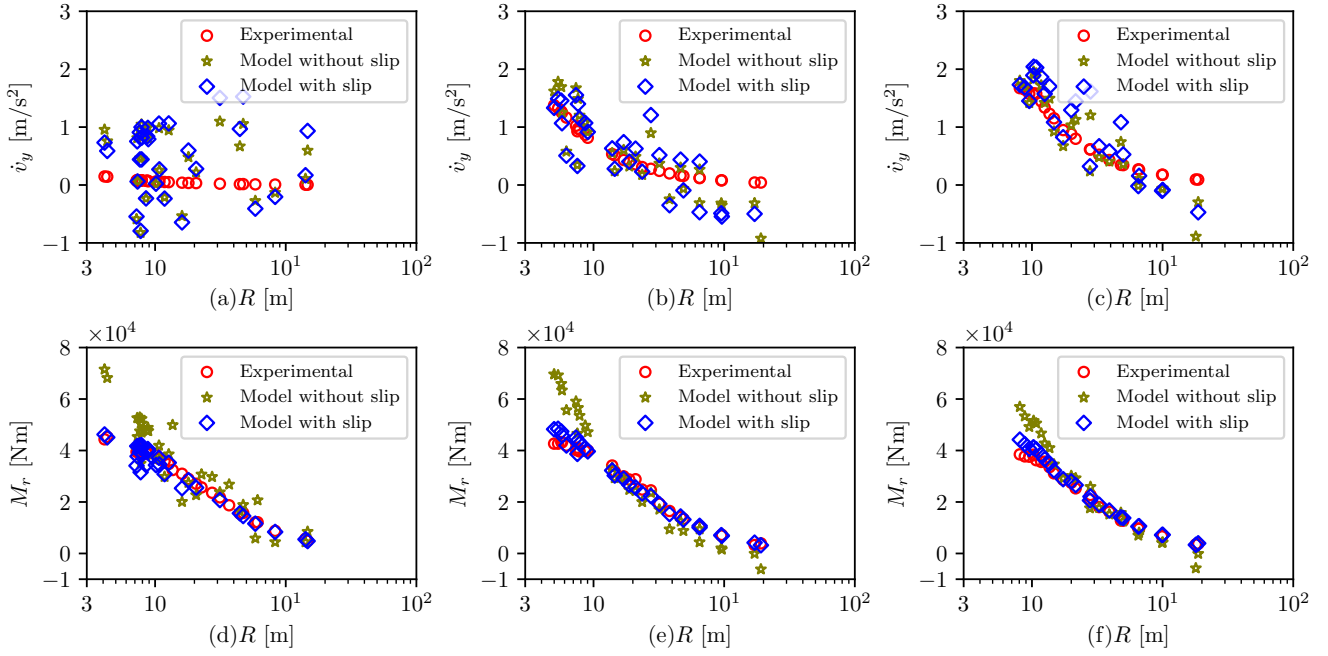
Fig. 11. Model verification on sand-gravel road at (a) and (d) 3 km/h, (b) and (e) 10 km/h, (c) and (f) 15km/h.
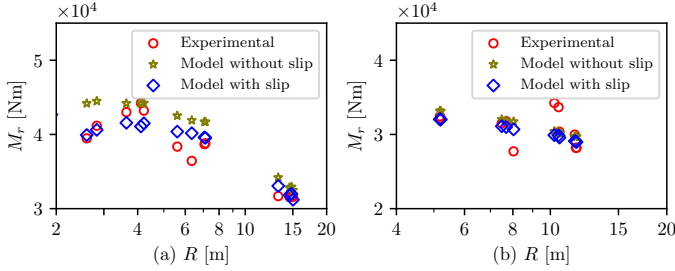

Fig. 12. Model verification on (a) firm soil road at 1.80-14.65 km/h and (b) cement road at 2.99-11.99 km/h.

limitations of test conditions and equipment, measuring the instantaneous accurate states is not feasible. However, using the average value from the steady-state turning process helps reduce the effect of the noise.

As shown in Fig. 11, the experimental results and model outputs of lateral acceleration and turning resistance moment on the sand-gravel road at different velocities are compared. The lateral acceleration collected was calculated from IMU data using $\dot{v}_y = v_x\gamma$, and the turning resistance moment was calculated from the motors' torque feedback. The model outputs are calculated by the proposed model Eq. (16), and the inputs of lateral velocity v_y and yaw rate γ are measured by the IMU system. The verification will be discussed in three aspects. In the first aspect, the model outputs considering longitudinal slip mostly agree with the experimental results in different velocities on the sand-gravel road. However, model outputs of lateral acceleration at 3 km/h (Fig. 11 a) show poor consistency with experimental results. The main reason is that the lateral velocity input to the model should be the lateral velocity of the unsprung part; however, we use the data from

the IMU system which is mounted on the body. Additionally, the lateral velocity is small at a low longitudinal velocity, and the lateral velocity measured by IMU may not be accurate enough due to the vehicle's vibration. Similar problems may also arise in the validation process of WV models on a rough road. Despite the noisy lateral velocity, the model outputs still show a sufficient trend with the experimental results at higher velocity, as the centrifugal force impedes the free swing of the body. In the second aspect, how does the simplification, such as weight transfer between two tracks and approximation in Eq. (13-15), influence the accuracy of the model? The impact of the simplification start to emerge around a turning radius of 10 meters, and the error of M_r increases as the turning radius reduces. Fortunately, the error is around 10% when the limit of the experimental TRV is reached, which is acceptable for control algorithm with robust. In the third aspect, our experimental results show that the longitudinal slip cannot be ignored for TRVs. If we assume $v_x^{t,ave}$ to be zero in Eq. (16), that is, ignoring the longitudinal slip, the error of M_r exceeds 60%, which is 6 times the error when considering the longitudinal slip. The mean absolute error (MAE) comparison of the models with or without considering slip ratio is shown in Table III. The MAE decreases as vehicle speed increases because higher velocity results in higher centrifugal force, which impedes the free swing of the body. While similar performance in lateral acceleration estimation is achieved, the MAE of the turning resistance moment estimated by the model considering the slip ratio is around 25% of that of the model not considering the slip.

Fig. 12 demonstrates that our model is efficient on different soil types. Metal tracks and metal tracks embedded with rubber are used in Fig. 12 (a) and Fig. 12 (b), respectively. Due to the limited data, we plotted points of different velocities on

State	Model	3km/h	10km/h	15km/h
M_r [Nm]	with slip	1819	1830	1559
	without slip	7002	8828	6038
$\dot{v}_y$ [m/s^2]	with slip	0.631	0.379	0.361
	without slip	0.582	0.324	0.258

the same figure, and only the turning resistance moment is verified. Our experimental results indicate that while lateral acceleration could be significantly affected by vehicle velocity, the turning resistance moment is not. Additionally, since lateral velocity having a limited effect on the turning resistance moment, it is ignored in the validation. As Fig. 12 shows, the model still maintains good fitting accuracy under different road conditions.

B. Comparing with existing control models

Existing control models for TRVs can be roughly categorized into three types: kinematic models, pure friction models, and empirical models. Among them, the kinematic model is the most widely used control model for TRVs, although it fails to impose dynamic constraints and relies on a lower controller to achieve desired kinematic states. However, it is not feasible to compare a kinematic model with a dynamic model.

The pure friction model neglects the relationship between the shear stress and shear displacement. It assumes that friction will reach its limit when relative displacement occurs, which does not conform to the terramechanics theory. As Fig. 13 shows, shear stress increases gradually with the shear displacement increasing until it reaches its limit, while the friction stress is a constant irrelevant to the relative displacement. To some extent, the pure friction theory can be regarded as a particular case of the Janosi-Hanamoto's equation when the shear deformation parameter K is infinitesimally small. Therefore, the pure friction model may work when the TRV travels on hard ground, like a small TRV on indoor hard floor, but models based on the terramechanics theory are more universal.
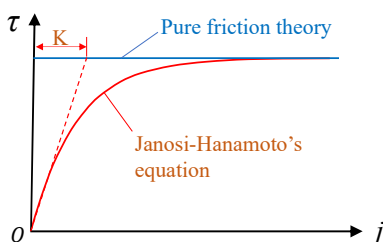

Fig. 13. Comparison between terramechanics theory and pure slip theory.

To further compare the model performance, a comparison between the proposed model and the pure friction model on a sand-gravel road at 15 km/h is made, as shown in Fig. 14. Even with parameters adjustments to fit the experimental data, the consistency between the pure friction model's prediction and experimental data is poor. The turning resistance moment

can easily reach its limit since the pure slip model neglects the shear displacement-shear displacement relationship. Therefore, the pure slip model does not apply to general off-road scenarios, but the proposed terramechanics-based dynamic model works well in such conditions.
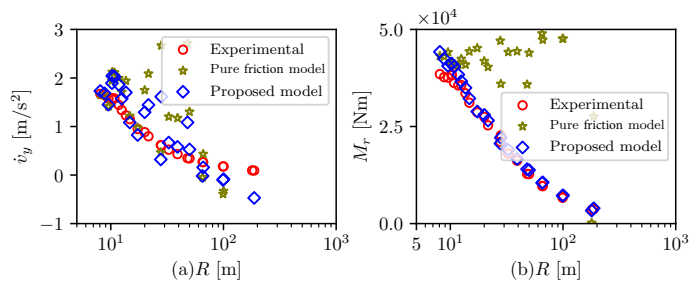

Fig. 14. (a) lateral acceleration and (b) turning resistance moment estimated by the proposed model and pure friction model on sand-gravel road at 15 km/h.

The empirical model, such as the Nikitin empirical formula, can be treated as an improved pure slip model. In the Nikitin empirical formula, the friction coefficient changes along with the turning radius, as Eq. (21) shows.

$$\mu = \frac{\mu_{max}}{a + (1-a)\frac{R+B/2}{B}} \tag{21a}$$

$$M_r = \frac{1}{4}GL\mu \tag{21b}$$

where, a is a parameter, and $a = 0.85$ is recommended. μ is turning resistance coefficient. μ_{max} is the turning resistance coefficient when the turning radius is $B/2$. The Nikitin empirical formula assumes the project of turning center O_c is always located on the CoG, implying the vehicle velocity v is always forward. That is, the lateral dynamic is neglected. In other words, the Nikitin empirical formula can only be used to estimate the turning resistance moments, that is, the yaw dynamics. To compare the model performance, we fitted the Nikitin empirical with the experimental data to its best performance by adjusting the parameters of μ_{max} and a, as Fig. 15 shown. The MAE performance comparison between the proposed model and the Nikitin empirical formula is shown in Table IV. The two models achieve similar performances, but the Nikitin formula is an empirical formula that neglects the lateral dynamics. In addition, the parameters in the Nikitin formula do not have a clear physical meaning. Therefore, compared to the Nikitin empirical formula-based models, the proposed terramechanics-based model includes lateral dynamics and has a clear physical meaning while achieving similar performance in estimating the turning resistance moment.

TABLE IV
THE MAE COMPARISON BETWEEN THE PROPOSED MODEL AND THE
NIKITIN EMPIRICAL FORMULA ON SAND-GRAVEL ROAD.

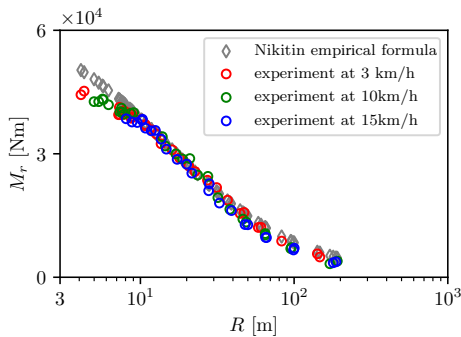| State	Model	3km/h	10km/h	15km/h
M_r [Nm]	Proposed model	1819	1830	1559
	Nikitin	1441	1870	1374

Fig. 15. Experimental data and the Nikitin empirical formula fitted performance.

C. Simulation

To further verify the effectiveness of the proposed control scheme and strategy, simulations were conducted on the MAT-LAB/Simulink and Recurdyn multibody dynamic software co-simulation. Different scenarios, including lane change scenario and steady turning scenario, were introduced to validate the proposed method. As indicated in Section II-A, the kinematic model and empirical model are the most commonly used models for path tracking of TRVs. Thus, these two models were used as comparison models to verify the effectiveness of the proposed model. The kinematic model calculates the desired sprocket speeds with an MPC controller, and these speeds are fulfilled by PID controllers. The empirical model used for comparison is shown as following:

$$\dot{\gamma} = \frac{M_t}{I_z} - \frac{GL}{4I_z} \frac{\mu_{\max}}{a + (1-a)\frac{v_x/\gamma + B/2}{B}} \qquad (22)$$

For the empirical and proposed models, the control frequency was 10 Hz, and the predictive horizon and control horizon were set as 10 and 3, respectively. Since the kinematic model is relatively simple, its control frequency was set as 100 Hz, with a predictive horizon of 20, and a control horizon of 4.

Fig. 16 shows the results of the system states with different models and control schemes during the lane-change maneuver. As shown in Fig. 16 (a), all the models can follow the desired trajectory, but the proposed model and control scheme exhibit the best performance. Detailed states of the TRV during lane change maneuver, including longitudinal velocity, yaw rate, tracking errors, etc., are shown in Fig. 16 (b)-(g). From 16 (b), it can be seen that all the methods can follow a desired longitudinal velocity, but the empirical model and the proposed model perform better. Fig. 16 (e) and 16 (f) show that the proposed model and scheme have minimal control error in lane-change maneuver. Fig. 16 (d) and (g) show the outputs of the MPC controller and the final torque output of the left sprocket. The final torque output of the kinematic model does not appear as stable as that of the empirical model and the proposed model. This instability is mainly because the Kinematic model follows the desired path by controlling the sprocket speed; however, the sprocket is directly engaged with the track, resulting in noisier states. Thus, dynamic models

result in more stable vehicle states and reduced corresponding actuator demands.

As mentioned, the small turning radius of the TRVs can lead to modeling errors for both the dynamic model and the kinematic model. Therefore, path following for steady-state turning on small turning radius was used to verify the effectiveness of the proposed model. Fig. 17 shows the results of steady-state turning with a radius of 10 meters. Compared with the kinematic and empirical models, the proposed model has the lowest tracking error and one of the most stable states, as Fig. 17 (e)-(f) illustrates. It should be noted that the torque output of the kinematic model is extremely unstable, which is difficult to achieve in the real world, as Fig. 17 (g) shows. The path-following performance comparison between our proposed method and previous methods is shown in Table V. In summary, the proposed method has the best comprehensive control performance.

TABLE V
THE MAE COMPARISON BETWEEN MODELS AND SCENARIOS.

Model	lane change		steady turn	
	$y_{\mathrm{err}}(\mathrm{m})$	$\varphi_{\mathrm{err}}(\mathrm{rad})$	$y_{\mathrm{err}}(\mathrm{m})$	$\varphi_{\mathrm{err}}(\mathrm{rad})$
empirical	0.0548	**0.0067**	0.1799	0.0570
kinematic	0.0353	0.0135	0.2697	**0.0541**
proposed	**0.0221**	0.0081	**0.0905**	0.0566

VI. CONCLUSION

In this paper, we propose a terramechanics-based TRV dynamics model that avoids complex integration and can be used in optimization-based real-time control for the first time. By introducing concepts of slip ratio and slip angle from the field of WVs, we have derived a concise track-ground interaction model. To reduced measurement demands, we simplified the TRV model to a single-track model and designed an efficient motion control scheme by considering lateral and longitudinal dynamics separately. The dynamic model was verified through the real car experimental results, and the control scheme was validated with multibody dynamics simulations. The results show that the proposed dynamic model is consistent with the real-car experiments, and the proposed control scheme can improve the performance of TRV path following tasks.

While the proposed single-track dynamic model demonstrates its advantages, it still has some limitations. Although the proposed model is validated on regular firm soil, it may will not perform well on soft ground due to the limitation of the Janosi-Hanamoto's equation (Eq. 2). The equation does not consider the bulldozing force; however, the bulldozing force will replace the shear force as the main form of resistance when tracks sink into soft soil.

REFERENCES

[1] Z. Zang, J. Gong, Z. Li, J. Song, H. Liu, C. Gong, X. Zhang, and Y. Li, "Formation trajectory tracking control of utvs: A coupling multi-objective iterative distributed model predictive control approach," *IEEE Transactions on Intelligent Vehicles*, 2022.

[2] B. Janarthanan, C. Padmanabhan, and C. Sujatha, "Lateral dynamics of single unit skid-steered tracked vehicle," *International Journal of Automotive Technology*, vol. 12, no. 6, pp. 865–875, 2011.
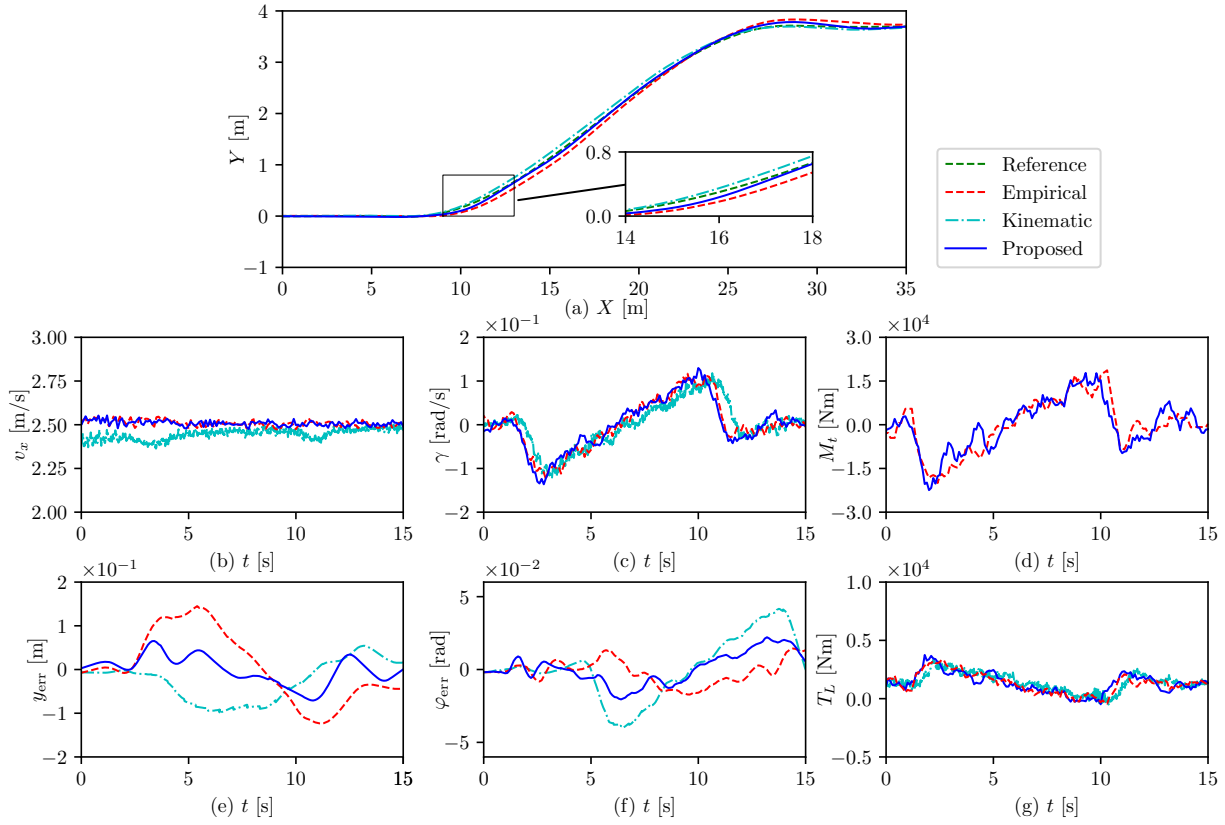
Fig. 16. System states of (a) position, (b) longitudinal velocity, (c) yaw rate, (d) driving moment, (e) lateral error, (f) yaw angle error and (g) left sprocket torque output comparison in lane change maneuver.
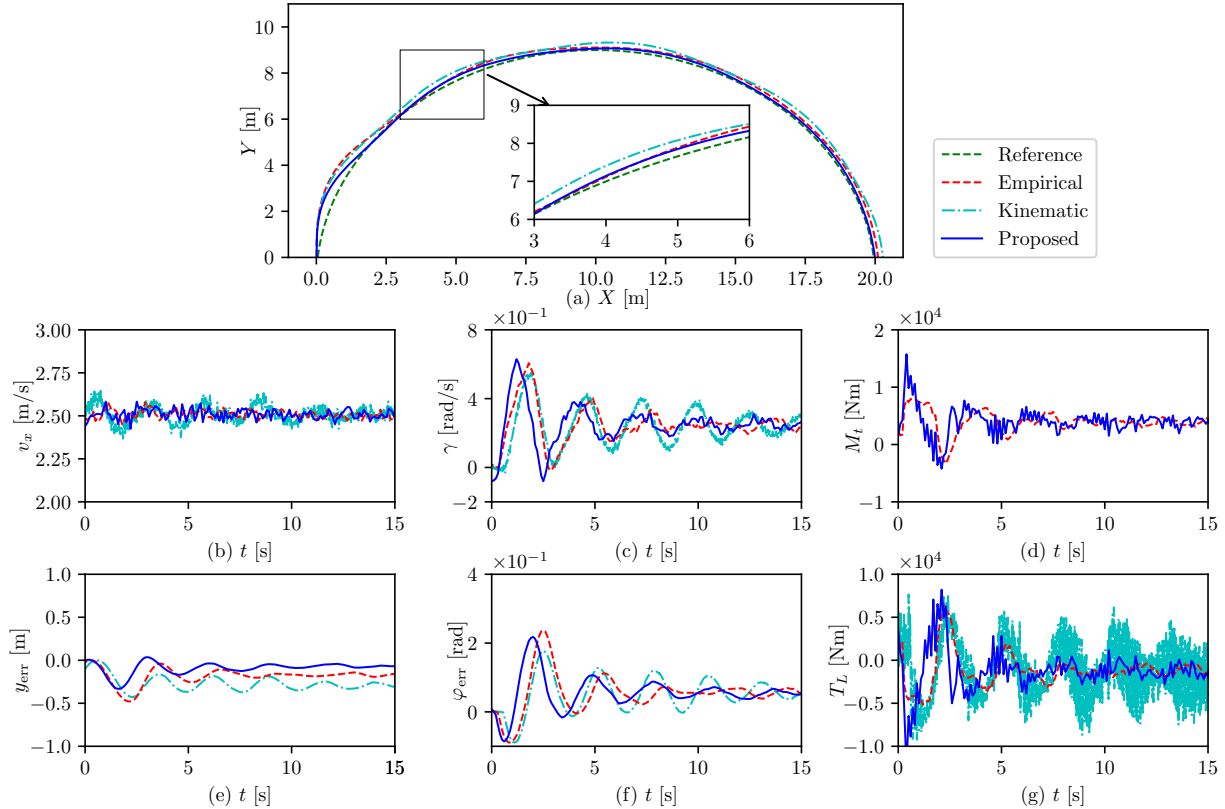

Fig. 17. System states of (a) position, (b) longitudinal velocity, (c) yaw rate, (d) driving moment, (e) lateral error, (f) yaw angle error and (g) left sprocket torque output comparison in steady-state turning maneuver.

[3] J. Y. Wong, C. Senatore, P. Jayakumar, and K. Iagnemma, "Predicting mobility performance of a small, lightweight track system using the computer-aided method ntvpm," *Journal of Terramechanics*, vol. 61, pp. 23–32, 2015.

[4] J. Wong, "Dynamics of tracked vehicles," *Vehicle system dynamics*, vol. 28, no. 2-3, pp. 197–219, 1997.

[5] T. Zou, J. Angeles, and F. Hassani, "Dynamic modeling and trajectory tracking control of unmanned tracked vehicles," *Robotics and Autonomous Systems*, vol. 110, pp. 102–111, 2018.

[6] B. Sebastian and P. Ben-Tzvi, "Physics based path planning for autonomous tracked vehicle in challenging terrain," *Journal of Intelligent & Robotic Systems*, vol. 95, no. 2, pp. 511–526, 2019.

[7] J. Yin, L. Li, Z. P. Mourelatos, Y. Liu, D. Gorsich, A. Singh, S. Tau, and Z. Hu, "Reliable global path planning of off-road autonomous ground vehicles under uncertain terrain conditions," *IEEE Transactions on Intelligent Vehicles*, 2023.

[8] M. T. Peterson, T. Goel, and J. C. Gerdes, "Exploiting linear structure for precision control of highly nonlinear vehicle dynamics," *IEEE Transactions on Intelligent Vehicles*, vol. 8, no. 2, pp. 1852–1862, 2022.

[9] K. Liu, J. Gong, A. Kurt, H. Chen, and U. Ozguner, "Dynamic modeling and control of high-speed automated vehicles for lane change maneuver," *IEEE Transactions on Intelligent Vehicles*, vol. 3, no. 3, pp. 329–339, 2018.

[10] Y. Huang, S. Z. Yong, and Y. Chen, "Stability control of autonomous ground vehicles using control-dependent barrier functions," *IEEE Transactions on Intelligent Vehicles*, vol. 6, no. 4, pp. 699–710, 2021.

[11] S. Yang, Y. Chen, R. Shi, R. Wang, Y. Cao, and J. Lu, "A survey of intelligent tires for tire-road interaction recognition toward autonomous vehicles," *IEEE Transactions on Intelligent Vehicles*, vol. 7, no. 3, pp. 520–532, 2022.

[12] Q. Shi and H. Zhang, "An improved control-oriented tire model and its applications on intelligent vehicles," *IEEE Transactions on Intelligent Vehicles*, 2023.

[13] H. B. Pacejka and E. Bakker, "The magic formula tyre model," *Vehicle system dynamics*, vol. 21, no. S1, pp. 1–18, 1992.

[14] K. Guo and D. Lu, "Unitire: unified tire model for vehicle dynamic simulation," *Vehicle System Dynamics*, vol. 45, no. S1, pp. 79–99, 2007.

[15] J. Y. Wong, *Terramechanics and off-road vehicle engineering: terrain behaviour, off-road vehicle performance and design*. Butterworth-heinemann, 2009.

[16] J. Wong, *Theory of ground vehicles*. John Wiley & Sons, 2008.

[17] Z. Zhao, H. Liu, H. Chen, J. Hu, and H. Guo, "Kinematics-aware model predictive control for autonomous high-speed tracked vehicles under the off-road conditions," *Mechanical Systems and Signal Processing*, vol. 123, pp. 333–350, 2019.

[18] X. Guang-ming, L. Hao, G. Kong-hui, and C. Hui-yan, "Research on trajectory prediction of tracked vehicles based on real time slip estimation (in chinese)," *Acta Armamentarii*, vol. 38, no. 3, p. 600, 2017.

[19] H. Jiaming, H. Yuhui, C. Huiyan, and L. Kai, "Research on trajectory tracking of unmanned tracked vehicles based on model predictive control (in chinese)," *Acta Armamentarii*, vol. 40, no. 3, p. 456, 2019.

[20] A. Nikitin and L. Sergeev, "Teoriya tanka [tank theory]," *Moscow, Izdaniye Akademii Bro-netankovykh voysk Publ*, 1962.

[21] J. Wong and C. Chiang, "A general theory for skid steering of tracked vehicles on firm ground," *Proceedings of the Institution of Mechanical Engineers, Part D: Journal of Automobile Engineering*, vol. 215, no. 3, pp. 343–355, 2001.

[22] X. Zhou, Z. Wang, H. Shen, and J. Wang, "Robust adaptive path-tracking control of autonomous ground vehicles with considerations of steering system backlash," *IEEE Transactions on Intelligent Vehicles*, vol. 7, no. 2, pp. 315–325, 2022.

[23] X. Shang and A. Eskandarian, "Emergency collision avoidance and mitigation using model predictive control and artificial potential function," *IEEE Transactions on Intelligent Vehicles*, vol. 8, no. 5, pp. 3458–3472, 2023.

[24] J. Lu, H. Liu, D. Li, H. Guan, Z. Li, and Z. Tang, "Research on lateral-longitudinal coupling trajectory tracking control method for bilateral electric drive tracked vehicle," in *2021 China Automation Congress (CAC)*. IEEE, 2021, pp. 3235–3240.

[25] M. Garber and J. Wong, "Prediction of ground pressure distribution under tracked vehicles—i. an analytical method for predicting ground pressure distribution," *Journal of Terramechanics*, vol. 18, no. 1, pp. 1–23, 1981.

[26] E. Bakker, L. Nyborg, and H. B. Pacejka, "Tyre modelling for use in vehicle dynamics studies," *SAE Transactions*, pp. 190–204, 1987.

[27] B. Maclaurin, "A skid steering model using the magic formula," *Journal of Terramechanics*, vol. 48, no. 4, pp. 247–263, 2011.

[28] H. Taghavifar and S. Rakheja, "A novel terramechanics-based path-tracking control of terrain-based wheeled robot vehicle with matched-mismatched uncertainties," *IEEE Transactions on Vehicular Technology*, vol. 69, no. 1, pp. 67–77, 2019.

[29] A. D. Sabiha, M. A. Kamel, E. Said, and W. M. Hussein, "Dynamic modeling and optimized trajectory tracking control of an autonomous tracked vehicle via backstepping and sliding mode control," *Proceedings of the Institution of Mechanical Engineers, Part I: Journal of Systems and Control Engineering*, vol. 236, no. 3, pp. 620–633, 2022.

[30] M. N. Özdemir, V. Kılıç, and Y. S. Ünlüsoy, "A new contact & slip model for tracked vehicle transient dynamics on hard ground," *Journal of Terramechanics*, vol. 73, pp. 3–23, 2017.

[31] S. Tang, S. Yuan, J. Hu, X. Li, J. Zhou, and J. Guo, "Modeling of steady-state performance of skid-steering for high-speed tracked vehicles," *Journal of Terramechanics*, vol. 73, pp. 25–35, 2017.

[32] J. Jiao, L. Sun, W. Kong, Y. Zhang, Y. Qiao, and C. Yuan, "A sliding parameter estimation method based on UKF for agricultural tracked robot," in *The 2014 2nd International Conference on Systems and Informatics (ICSAI 2014)*, 2014, pp. 277–282.

[33] Z. Li, L. Chen, Q. Zheng, X. Dou, and L. Yang, "Control of a path following caterpillar robot based on a sliding mode variable structure algorithm," *Biosystems Engineering*, vol. 186, pp. 293–306, 2019.

[34] H. Huang, L. Zhai, and Z. Wang, "A Power Coupling System for Electric Tracked Vehicles during High-Speed Steering with Optimization-Based Torque Distribution Control," *Energies*, vol. 11, no. 6, p. 1538, 2018.

[35] Z. Janosi, "The analytical determination of drawbar pull as a function of slip for tracked vehicles in deformable soils," in *Proc. of 1st Int. Conf. of ISTVS. Turin., 1961*, 1961.

[36] M. G. Bekker, "Theory of land locomotion," *(No Title)*, 1956.

[37] J. Wong, M. Garber, J. Radforth, and J. Dowell, "Characterization of the mechanical properties of muskeg with special reference to vehicle mobility," *Journal of Terramechanics*, vol. 16, no. 4, pp. 163–180, 1979.

[38] A. Nicolini, F. Mocera, and A. Soma, "Multibody simulation of a tracked vehicle with deformable ground contact model," *Proceedings of the Institution of Mechanical Engineers, Part K: Journal of Multi-body Dynamics*, vol. 233, no. 1, pp. 152–162, 2019.

[39] M. H. A. Sidi, K. Hudha, Z. A. Kadir, and N. H. Amer, "Modeling and path tracking control of a tracked mobile robot," in *2018 IEEE 14th International Colloquium on Signal Processing & Its Applications (CSPA)*, 2018, pp. 72–76.

[40] B. Sebastian and P. Ben-Tzvi, "Physics Based Path Planning for Autonomous Tracked Vehicle in Challenging Terrain," *Journal of Intelligent & Robotic Systems*, vol. 95, no. 2, pp. 511–526, 2019.

[41] S. Hong, J.-S. Choi, H.-W. Kim, M.-C. Won, S.-C. Shin, J.-S. Rhee, and H.-u. Park, "A path tracking control algorithm for underwater mining vehicles," *Journal of Mechanical Science and Technology*, vol. 23, no. 8, pp. 2030–2037, 2009.

[42] T. Zou, J. Angeles, and F. Hassani, "Dynamic modeling and trajectory tracking control of unmanned tracked vehicles," *Robotics and Autonomous Systems*, vol. 110, pp. 102–111, 2018.

[43] A. D. Sabiha, M. A. Kamel, E. Said, and W. M. Hussein, "Dynamic modeling and optimized trajectory tracking control of an autonomous tracked vehicle via backstepping and sliding mode control," *Proceedings of the Institution of Mechanical Engineers, Part I: Journal of Systems and Control Engineering*, vol. 236, no. 3, pp. 620–633, 2022.

[44] Y. Dai, C. Xue, and Q. Su, "An Integrated Dynamic Model and Optimized Fuzzy Controller for Path Tracking of Deep-Sea Mining Vehicle," *Journal of Marine Science and Engineering*, vol. 9, no. 3, p. 249, 2021.

[45] D. Cui, G. Wang, H. Zhao, and S. Wang, "Research on a Path-Tracking Control System for Articulated Tracked Vehicles," *Strojniški vestnik – Journal of Mechanical Engineering*, vol. 66, no. 5, pp. 311–324, 2020.

[46] A. D. Sabiha, M. A. Kamel, E. Said, and W. M. Hussein, "ROS-based trajectory tracking control for autonomous tracked vehicle using optimized backstepping and sliding mode control," *Robotics and Autonomous Systems*, vol. 152, p. 104058, 2022.

[47] R. Gonzalez, M. Fiacchini, T. Alamo, J. L. Guzman, and F. Rodriguez, "Adaptive Control for a Mobile Robot Under Slip Conditions Using an LMI-Based Approach," *European Journal of Control*, vol. 16, no. 2, pp. 144–155, 2010.

[48] T. Hiramatsu, S. Morita, M. Pencelli, M. Niccolini, M. Ragaglia, and A. Argiolas, "Path-Tracking Controller for Tracked Mobile Robot on Rough Terrain," *International Journal of Electrical and Computer Engineering*, vol. 13, no. 2, pp. 59–64, 2019.

[49] N. Strawa, D. I. Ignatyev, A. C. Zolotas, and A. Tsourdos, "On-Line Learning and Updating Unmanned Tracked Vehicle Dynamics," *Electronics*, vol. 10, no. 2, p. 187, 2021.

[50] M. A. Subari, K. Hudha, Z. A. Kadir, S. M. Fairuz Syed Mohd Dardin, and N. H. Amer, "Development of Path Tracking Controller for An Autonomous Tracked Vehicle," in *2020 16th IEEE International Colloquium on Signal Processing & Its Applications (CSPA)*, 2020, pp. 126–130.

[51] Q.-j. Han and S.-j. Liu, "Path tracking control of tracked vehicle," *International Journal of Computer Science Issues (IJCSI)*, vol. 10, no. 6, p. 103, 2013.

[52] M. Ahmad, V. Polotski, and R. Hurteau, "Path tracking control of tracked vehicles," in *Proceedings 2000 ICRA. Millennium Conference. IEEE International Conference on Robotics and Automation. Symposia Proceedings (Cat. No.00CH37065)*, vol. 3, 2000, pp. 2938–2943 vol.3.

[53] J. Morales, J. L. Martínez, M. A. Martínez, and A. Mandow, "Pure-Pursuit Reactive Path Tracking for Nonholonomic Mobile Robots with a 2D Laser Scanner," *EURASIP Journal on Advances in Signal Processing*, vol. 2009, no. 1, p. 935237, 2009.

[54] M. A. Subari, K. Hudha, Z. A. Kadir, S. M. F. B. S. M. Dardin, and N. H. Amer, "Development of path tracking control of a tracked vehicle for an unmanned ground vehicle," *International Journal of Advanced Mechatronic Systems*, vol. 8, no. 4, pp. 136–143, 2020.

[55] J. Ni, Y. Wang, H. Li, and H. Du, "Path Tracking Motion Control Method Of Tracked Robot Based On Improved LQR Control," in *2022 41st Chinese Control Conference (CCC)*, 2022, pp. 2888–2893.

[56] H. Wu, Y. Chen, and H. Qin, "MPC Based Trajectory Tracking for An Automonous Deep-Sea Tracked Mining Vehicle," *ASP Transactions on Internet of Things*, vol. 1, no. 2, pp. 1–13, 2021.

[57] J. Gao and S. L. Zhang, "Path Tracking Control of Micro-Tracked Mobile Robot," *Applied Mechanics and Materials*, vol. 644–650, pp. 265–271, 2014.

[58] X. Wang, J. Taghia, and J. Katupitiya, "Robust Model Predictive Control for Path Tracking of a Tracked Vehicle with a Steerable Trailer in the Presence of Slip," *IFAC-PapersOnLine*, vol. 49, no. 16, pp. 469–474, 2016.

[59] D. Li, S. Wu, Y. Zhao, Z. Li, and J. Gong, "A hierarchical path tracking method for high-speed unmanned tracked vehicle," in *2021 IEEE International Intelligent Transportation Systems Conference (ITSC)*. IEEE, 2021, pp. 38–43.

[60] Z. Zhao, H. Liu, H. Chen, J. Hu, and H. Guo, "Kinematics-aware model predictive control for autonomous high-speed tracked vehicles under the off-road conditions," *Mechanical Systems and Signal Processing*, vol. 123, pp. 333–350, 2019.

[61] M. Burke, "Path-following control of a velocity constrained tracked vehicle incorporating adaptive slip estimation," in *2012 IEEE International Conference on Robotics and Automation*, 2012, pp. 97–102.

[62] S. Tang, S. Yuan, J. Hu, X. Li, J. Zhou, and J. Guo, "Modeling of steady-state performance of skid-steering for high-speed tracked vehicles," *Journal of Terramechanics*, vol. 73, pp. 25–35, 2017.

[63] K. Berntorp, R. Quirynen, T. Uno, and S. Di Cairano, "Trajectory tracking for autonomous vehicles on varying road surfaces by friction-adaptive nonlinear model predictive control," *Vehicle System Dynamics*, vol. 58, no. 5, pp. 705–725, 2020.

[64] D. Tavernini, M. Metzler, P. Gruber, and A. Sorniotti, "Explicit nonlinear model predictive control for electric vehicle traction control," *IEEE Transactions on Control Systems Technology*, vol. 27, no. 4, pp. 1438–1451, 2018.

[65] M. Brown and J. C. Gerdes, "Coordinating tire forces to avoid obstacles using nonlinear model predictive control," *IEEE Transactions on Intelligent Vehicles*, vol. 5, no. 1, pp. 21–31, 2019.

[66] M. Ataei, A. Khajepour, and S. Jeon, "Model predictive control for integrated lateral stability, traction/braking control, and rollover prevention of electric vehicles," *Vehicle system dynamics*, vol. 58, no. 1, pp. 49–73, 2020.

BIOGRAPHY SECTION

Ruizeng Zhang received the B.E. degree from Shandong University, Jinan, China, in 2016. He is currently working toward the Ph.D. degree with the School of Mechanical Engineering, Beijing Institute of Technology. He was a Visiting Scholar with the Mechatronic Vehicle Systems Lab, University of Waterloo from 2021 to 2023. His main research interest are motion control and planning of autonomous vehicle system.
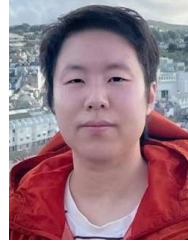
Wei Zhou is an Assistant Professor at Cardiff University, United Kingdom. Dr Zhou was a Postdoctoral Fellow at University of Waterloo, Canada. Wei received the Ph.D. degree from the University of Science and Technology of China in 2021, joint with the University of Waterloo from 2019 to 2021.

Dr Zhou was a visiting scholar at National Institute of Informatics, Japan, a research assistant with Intel, and a research intern at Microsoft Research and Alibaba Cloud. Wei is now an Associate Editor of IEEE Transactions on Neural Networks and Learning Systems. Wei's research interests span multimedia computing, perceptual image processing, and computational vision.

Haiou Liu received the B.S. and Ph.D. degrees from the Beijing Institute of Technology, Beijing, China, in 1998 and 2003, respectively. She is currently a Professor with the School of Mechanical Engineering, Beijing Institute of Technology. Her teaching interest focuses on vehicle control classes at both undergraduate and graduate levels. Her research interests include design and control of automated manual transmission and hybrid powertrain.

Jianwei Gong received the B.S. degree from the National University of Défense Technology, Changsha, China, in 1992, and the Ph.D. degree from the Beijing Institute of Technology, Beijing, China, in 2002. From 2011 to 2012, he was a Visiting Scientist with the Robotic Mobility Group, Massachusetts Institute of Technology, Cambridge, MA, USA. He is currently a Professor and the Director of the Intelligent Vehicle Research Centre, School of Mechanical Engineering. His research interests include intelligent vehicle environment perception and understanding, decision making, path/motion planning, and control.

Huiyan Chen received the Ph.D. degree from the Beijing Institute of Technology, Beijing, China, in 2004. Since 1981, he has been with the Beijing Institute of Technology, where he is currently a Professor with the Intelligent Vehicle Research Center. His research interests include intelligent vehicle and vehicle automatic transmission technologies.

Amir Khajepour is a Professor of mechanical and mechatronics engineering with the University of Waterloo, Waterloo, ON, Canada, and the Canada Research Chair in Mechatronic Vehicle Systems. He has developed an extensive research program that applies his expertise in several key multidisciplinary areas. His research interests include system modeling and control of dynamic systems. His research has resulted in several patents and technology transfers. He is the author of more than 350 journal and conference publications and five books. He is a Fellow of the Engineering Institute of Canada, the American Society of Mechanical Engineers, and the Canadian Society of Mechanical Engineering.